CHARACTERIZATION OF BIFACIAL TECHNOLOGY PV SYSTEMS

S. Moreno-Buesa*[,1], E. Muñoz-Cerón[1], G. Nofuentes[1], S. Gulkowski[2], J. de la Casa[1], J. Aguilera[1]

*Corresponding author. E-mail: smmoreno@ujaen.es

[1] PV IDEA Research Group (Research and Development in Solar Energy). University of Jaén, Spain

[2] Lublin University of Technology, Poland

Keywords: *Photovoltaic systems, bifacial, rear irradiance, performance analysis*

ABSTRACT: Bifacial solar technology has experienced exponential growth in recent years and its trend is increasing for the coming years. Considering the advantages that it offers over monofacial technology such as its current price equivalence, the increase in performance thanks to the production of the rear face and the consecutive reduction of the LCOE, it is logical that more and more photovoltaic plants with this technology are been installed. Nowadays, there are some regulatory gaps regarding bifacial technology and, due to this growing trend, it is necessary to study, research and implement the optimal way to evaluate these systems. This article has experimented with a 3.3 kW bifacial photovoltaic system, divided into two strings with different configurations, whose monitoring system has all the instrumentation included in the IEC 61724 standard, with the addition that it has several rear irradiance sensors arranged in different locations of the system to evaluate the variability of this parameter. After an experimental campaign of nine months, a power estimation analysis and the calculation of the PR and $PR_{25°C}$ have been carried out using the different rear irradiance sensors. The variability of this parameter depending on the location of the sensor has affected the results in such a way that the RMSE committed in the power estimation has varied between 10.22% and 2.63%,

while the PR and $PR_{25ºC}$ of the system has oscillated between 0.84 for the most unfavorable case and 0.95 in the most favorable case. Assumed the great variability between performance ratios, it is necessary to establish a specific normative standard for the evaluation of Bifacial PV systems.

1. INTRODUCTION

Due to the energy transition [1], [2] and photovoltaic expansion in which we have been immersed for some time, there have been many efforts to optimize the generation of solar energy aiming to obtain maximum energy from the minimum space.

As a consequence, an emerging technology such as bifacial technology begins to stand out, whose basic principle lies in the ability to produce electrical energy from both sides of the cell.

Having overcome the price barrier of the technology, equating its price with monofacial technology, it has taken great relevance on the market share. Nowadays, in 2023, bifacial modules occupy the 70% of the global market and it is expected that by 2033 they will reach 90% of the market share [3]. As a result of the price reduction, research on this technology has increased in order to understand its behavior and to define well the new variables involved, as well as how to characterize them.

Since 1980, research has been done on the energy gains that bifacial technology can have thanks to albedo [4], [5] but most experimental studies date from more recent dates. At the physical level of cell, the behavior of different materials has been studied [6], [7] and its efficiency has been maximized, reaching values of 32.5% [8]. Other studies compare the profitability of bifacial versus monofacial systems, exposing the variation of the parameter that may exist for bifacial installations depending on the albedo [9], [10].

One of the main problems is the characterization of albedo irradiance and its homogeneity, which depends in one hand on the height of the modules as much as the arrangement and in the other hand on the materials of the albedo surface [11]–[13]. One proven way to maximize the gain of a BPV systems is the use of solar trackers [14], [15]. It is therefore important to implement irradiance models for bifacial modules with which reliable production estimates can be made [16], [17]. Nowadays, there is a lack of experimental data due to a relevant number of publications are based on simulations, but for the achievement of this purpose it is necessary to research operating and performance data.

Regarding the scope of integration, the studies carried out try to occupy spaces not usable for the performance of activities, such as installations in irrigation reservoirs or water bodies (FPV) [18], [19] or the use of rooftops [20]–[22]. Agrovoltaics (APV) is an example in which it is integrated into spaces that coexist with the development of agricultural activity[23]–[25]. Considering the production capacity on both sides, it is interesting to study its behavior in vertical arrangement [26], [27].

With the expansion of bifacial modules, the new parameters that affect to the performance has to be considered, such as bifaciality coefficients and bifacial gain [28]. The current regulations do not facilitate the characterization of these modules, since unlike monofacial technology, outdoor characterization is not established, but indoor [29], [30].

Problems arise when monitoring a BPV system, since the existing standard only refers to the measurement of the rear irradiance in an appendix to IEC 61724-1 [31]. By not specifying the position of the rear irradiance sensor in the installation, considering the variability of the albedo, there is no standard for the measurements of bifacial systems to be carried out under similar conditions and the evaluation of the yields to be completely reliable. In the literature review, there are a variety of articles on estimates based on algorithms and models [32], but almost anyone where real performance data is offered.

As an example, there are studies that compares the performance of monofacial modules against bifacial modules as monofacial but the fact of not considering the effect of albedo irradiance on the bifacial implies the obtaining of uncertainty results because of the ratio of energy generation and irradiation received is not representative, obtaining a higher performance than in the case of bifacial [33].

Beyond the evaluation of a system correcting the performance ratio in degradation [34], this article shows the differences that may exist due to the variability exposed on the measurement of the rear irradiance depending on the position of the sensors, lengths of arrays and the parameters that affect this component. In this way, it is proposed to give visibility to the lack of a standard that allows the goodness indices that show the performance of BPV systems to be equivalent for all photovoltaic installations.

2. EXPERIMENTAL SETUP AND METHODOLOGY

For the development of the experiments, an experimental setup has been designed and put into operation, which is located on the north terrace of the Higher Polytechnic School of Jaén, Spain.

2.1 Bifacial photovoltaic system

The photovoltaic system consists of eight 410 W bifacial modules facing South and tilted 30 degrees, divided into two strings with different arrangements and connected to both MPPT's of the 3.3 kW inverter.

String 1 is composed of four bifacial modules arranged in a single line array, while string 2, composed of four other bifacial modules, is divided into two structures with two modules each one. Different configurations can allow observing differences in behavior depending on the length of the array. It should be noted that the structures used have been optimized as far as possible to avoid shading in the modules and have a telescopic floor to modify the height of the modules with respect to the albedo surface. Figure 1 show the arrangement of the bifacial photovoltaic system.

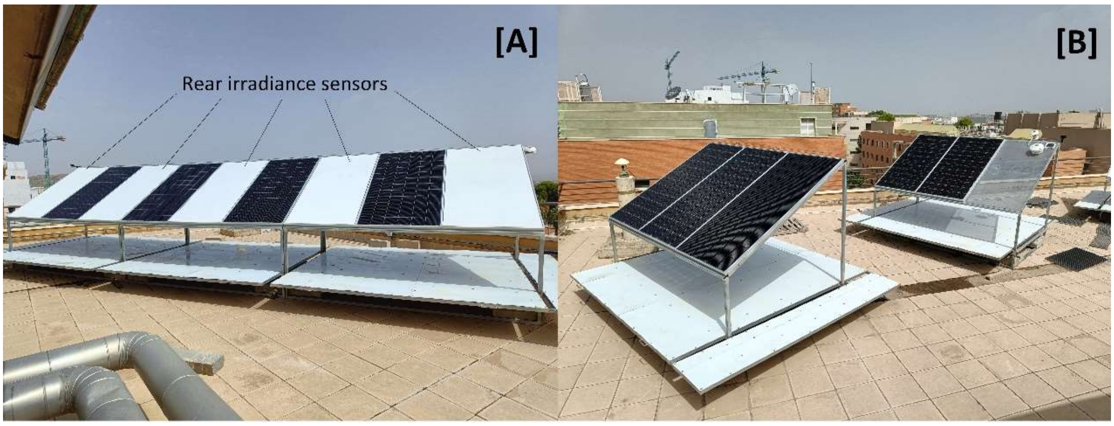

Figure 1: [A] String 1 arrangement. [B] String 2 arrangement

2.2 Monitoring system

The monitoring system, that allows the data collecting of the most relevant parameters for analysis, has been dimensioned complying with the IEC 61724-1 standard [31]. The monitoring system has been designed for the experimental purposes of understanding how the new variables that affect bifacial modules evolve, such as rear irradiance of albedo, and how it can be characterized [35].

In the same way as for monofacial systems, there are a weather vane and an anemometer for the measurement of wind speed and direction, K-type thermocouples for the measurement of module temperature and another thermocouple shady for the measurement of ambient temperature, a front and a rear spectroradiometer in order to measure spectral wave of frontal radiation and rear albedo and for the measurement of frontal irradiance there are two pyranometers, a calibrated cell and a calibrated module.

Regarding the variables that affect the rear face, several calibrated modules have been arranged whose front face has been covered with vinyl to use them as rear irradiance sensors so that each power module is inserted between two sensors as shown in Figure

1[A], allowing to observe how this parameter evolves along the string. Table 1 shows the notation of the irradiance sensors used for the analysis.

Table 1: Notation of the different irradiance sensors

Name	Sensor type	Position	Description
GF	Pyranometer	String 1	Frontal irradiance sensor
Galb	Albedometer	String 2	Rear global irradiance sensor
GR1	Calibrated module	String 1 (West side)	Rear irradiance sensor
GR3	Calibrated module	String 1 (Central-West side)	Rear irradiance sensor
GR5	Calibrated module	String 1 (Centre)	Rear irradiance sensor
GR7	Calibrated module	String 1 (Central-East side)	Rear irradiance sensor
GR9	Calibrated module	String 1 (East side)	Rear irradiance sensor

All sensors have been connected to a datalogger able to providing a daily file with the measurements made every minute during the nine months of the experimental campaign, corresponding to a Class A monitoring system [31]. Figure 2 provides a top view of the system, pointing the location of the most relevant elements of the system.

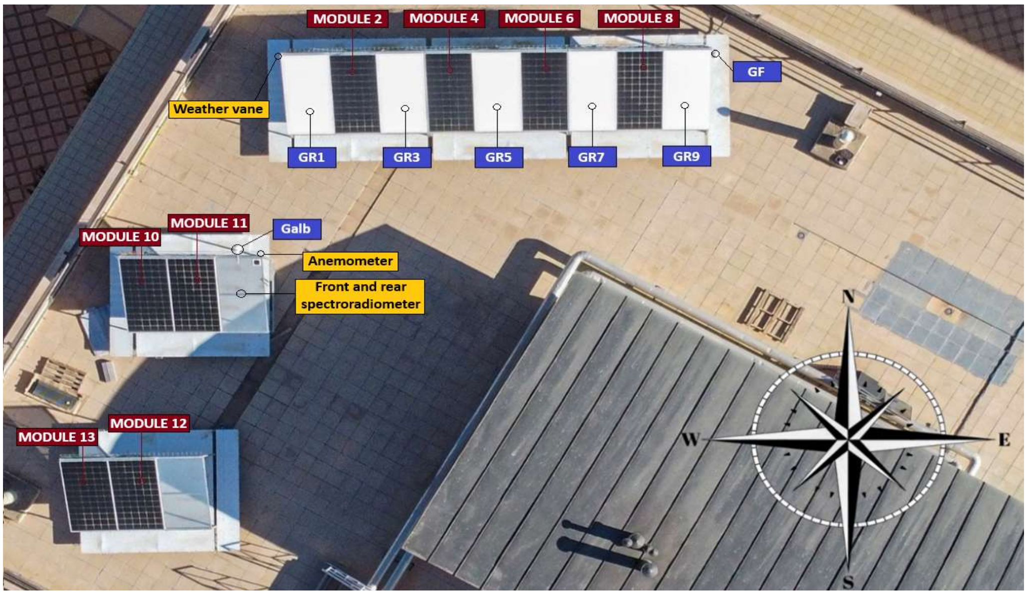

Figure 2: Top view of the system, pointing the location of the modules and the sensors

2.3 Bifacial module characterization campaign

Within the campaign to fine-tune the system an in order to ensure that the data obtained in the analyses are as close to reality as possible, a characterization campaign of the modules have been carried out to obtain the real operating parameters. To carry out this purpose, two modules of the same brand and same model have been transferred to the Centre for Energy, Environmental and Technological Research (CIEMAT), an accredited independent laboratory located in Madrid empowered to grant calibration certificated that reflect the electrical parameters of both sides of the modules measured in STC, thus obtaining two modules to use as a measurement standard.

Independently, the faces of each modules that make up the photovoltaic generator have been measured together with a calibrated standard module, ensuring that being under the same conditions of temperature and irradiance, the values of the calibrated module can be extrapolated [36] to the module to be characterized by equation 1:

$$\frac{{P_{eval}}^{STC}}{P_{eval}} = \frac{{P_{CIEMAT}}^{STC}}{P_{CIEMAT}} \qquad (1)$$

Where ${P_{eval}}^{STC}$ is the power in STC that we want to obtain from the module to be calibrated, P_{eval} corresponds to the measured power of the module to be characterized, P_{CIEMAT} represents the value of the measured power of the standard module and ${P_{CIEMAT}}^{STC}$ the value of the power in STC conditions of the standard module.

After analysing the results, modules whose power difference is smaller with respect to the standard has been separated to be used as rear irradiance sensors and those whose power is similar to group them in both strings so that the power of a module of greater power delivery is not limited by another of lower performance. Finally, the system has a characterized power of 3.621 kW, in which 1.64 kW belong to string 1 and 1.621 kW to string 2.

2.4 Methodology

The setup under study has been monitored throughout an experimental campaign from October 2022 to June 2023. The data obtained have been treated and processed in order to perform the following analyses:

- **Albedo rear irradiance analysis:** For a sunny day and a cloudy day, a posterior irradiance map has been prepared along string 1 with the intention of visualizing the evolution of irradiance. Similarly, the homogeneity of the rear irradiance of albedo along the same string has been analysed using the GNU index.
- **Estimation of the power generation:** As a representative, a day of good weather conditions and a cloudy day have been selected and, using a theoretical model applied to bifacial conditions, the daily power curve has been calculated for each rear irradiance sensor in order to verify which of them best fits the real measured power curve.
- **Evaluation of the performance of the system:** The existing differences that can occur for the measurement of the indices of goodness, such as the PR and the $PR_{25°C}$, have been evaluated depending on the parameters used for their measurement, as well as mainly the location of the sensors for measuring rear irradiance.

3. RESULTS

3.1 Albedo rear irradiance analysis

Since in string 1 the rear irradiance sensors are located on both sides of each generator module, it has been decided to make the arithmetic mean between the sensors adjacent to each module to obtain four more measurements of fictitious irradiance corresponding to the one that would occupy the position of each module, so that we would have the irradiance GR2 on the position of module 2, GR4 on the position of module 4, GR6 on the position of module 6 and GR8 on the position of module 8.

Figure 3 shows the rear irradiance curves for a sunny day and a cloudy day.

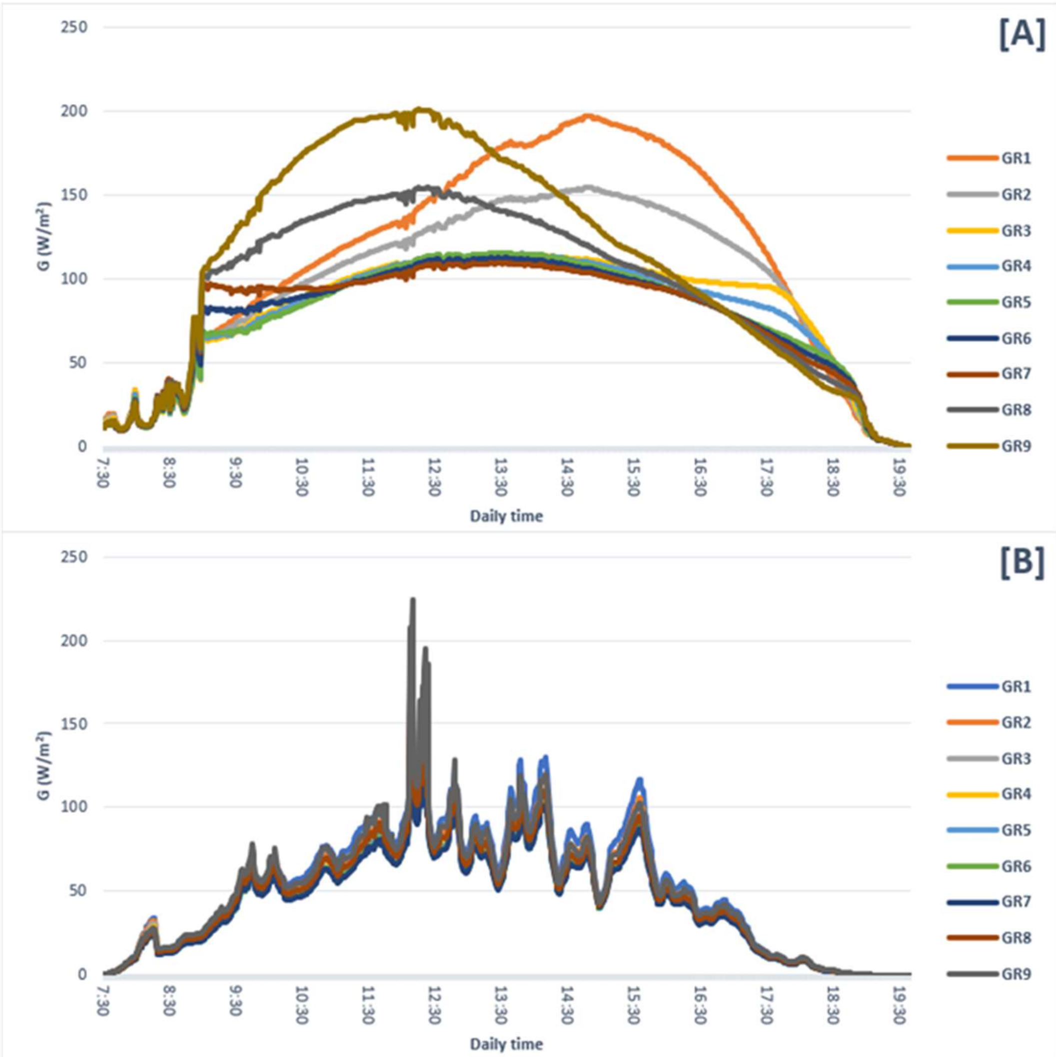

Figure 3: Evolution of the rear irradiance of albedo measured by each sensor. [A] Throughout a sunny day. [B] Throughout a cloudy day

On a sunny day, it is observed that there is a symmetry with respect to the central axis of the array, so that the extreme sensors on the East side (GR9 and GR8) collect much higher values than central sensors (from GR3 to GR7) in the morning hours and the extreme sensors on the West side (GR1 and GR2) act in the same way, but in the evening hours. However, on cloudy days, it can be seen that the difference between the measurements of the sensors is much smaller [37].

A rear irradiance map has been prepared that graphically shows the hourly evolution of the irradiance for each sensor, as well as the homogeneity between the irradiance value along the array, shown in Table 2 for a sunny day and in Table 3 for a cloudy day.

Table 2: Rear irradiance map of string 1 throughout a sunny day

Time	GR1 W/m²	GR2 W/m²	GR3 W/m²	GR4 W/m²	GR5 W/m²	GR6 W/m²	GR7 W/m²	GR8 W/m²	GR9 W/m²
8:30	19.95	19.58	19.21	19.50	19.80	20.89	21.99	22.03	22.08
9:30	77.63	73.32	69.00	69.10	69.20	81.14	93.09	111.16	129.23
10:30	104.23	96.77	89.30	86.84	84.39	89.33	94.27	134.22	174.17
11:30	126.51	115.45	104.38	102.79	101.19	99.88	98.57	147.10	195.64
12:30	149.48	131.06	112.64	113.19	113.74	110.95	108.17	152.73	197.29
13:30	178.24	146.49	114.74	114.75	114.76	111.80	108.85	139.76	170.68
14:30	192.06	151.97	111.88	111.27	110.67	107.78	104.89	125.09	145.29
15:30	188.60	147.33	106.07	103.33	100.60	98.99	97.39	106.63	115.88
16:30	163.56	130.89	98.23	92.20	86.18	86.39	86.60	88.50	90.40
17:30	113.99	104.59	95.20	82.50	69.80	68.09	66.39	63.73	61.08
18:30	39.29	44.71	50.13	50.15	50.17	46.86	43.56	38.27	32.98
19:30	0.60	0.64	0.67	0.64	0.60	0.59	0.59	0.69	0.79

Table 3: Rear irradiance map of string 1 throughout a cloudy day

Time	GR1 W/m²	GR2 W/m²	GR3 W/m²	GR4 W/m²	GR5 W/m²	GR6 W/m²	GR7 W/m²	GR8 W/m²	GR9 W/m²
8:30	15.28	14.72	14.15	13.86	13.57	13.19	12.81	14.52	16.23
9:30	45.16	42.93	40.69	40.27	39.85	40.06	40.27	44.61	48.95
10:30	57.69	53.61	49.54	48.87	48.21	47.57	46.93	50.86	54.80
11:30	93.09	85.76	78.43	78.17	77.90	76.95	75.99	84.55	93.11
12:30	81.52	76.90	72.28	71.94	71.59	71.43	71.27	75.25	79.23
13:30	68.05	63.76	59.48	58.28	57.08	56.64	56.19	59.77	63.35
14:30	81.69	74.04	66.39	65.49	64.59	63.97	63.35	68.33	73.30
15:30	110.19	99.41	88.63	87.57	86.52	84.79	83.07	90.01	96.95
16:30	38.17	35.13	32.10	31.66	31.23	30.61	29.99	33.06	36.13
17:30	12.69	11.87	11.04	10.89	10.75	10.43	10.11	11.38	12.65
18:30	1.99	1.96	1.94	1.86	1.79	1.74	1.68	2.02	2.36
19:30	0.00	0.00	0.00	0.00	0.00	0.00	0.00	0.00	0.00

Finally, the optical homogeneity index has been calculated by equation 2:

$$\boldsymbol{GNU} = \frac{\mathbf{max}(\boldsymbol{GR}_{\mathbf{1-9}}) - \mathbf{min}(\boldsymbol{GR}_{\mathbf{1-9}})}{\mathbf{max}(\boldsymbol{GR}_{\mathbf{1-9}}) + \mathbf{min}(\boldsymbol{GR}_{\mathbf{1-9}})}\ (\%) \qquad (\mathbf{2})$$

This index shows the percentage difference between the value of the array sensors for each moment of the day, being closer to zero the greater homogeneity [38]. Figure 4 shows the daily variation of this index on a sunny day and a cloudy day.

Figure 4: Evolution of GNU throughout a sunny day and a cloudy day

On cloudy days, although the measured values are lower, it is distributed more homogeneously along the string maintaining differences between 5% and 15%. On the contrary, on sunny days there are differences of up to 35% in the rear irradiance peaks for the central hours of the morning and afternoon.

3.2 Estimation of the power generation

The first consideration for this analysis is that, when representing the power measured curve throughout the entire day, there is shading caused by a building early in the morning, as shown in Figure 5.

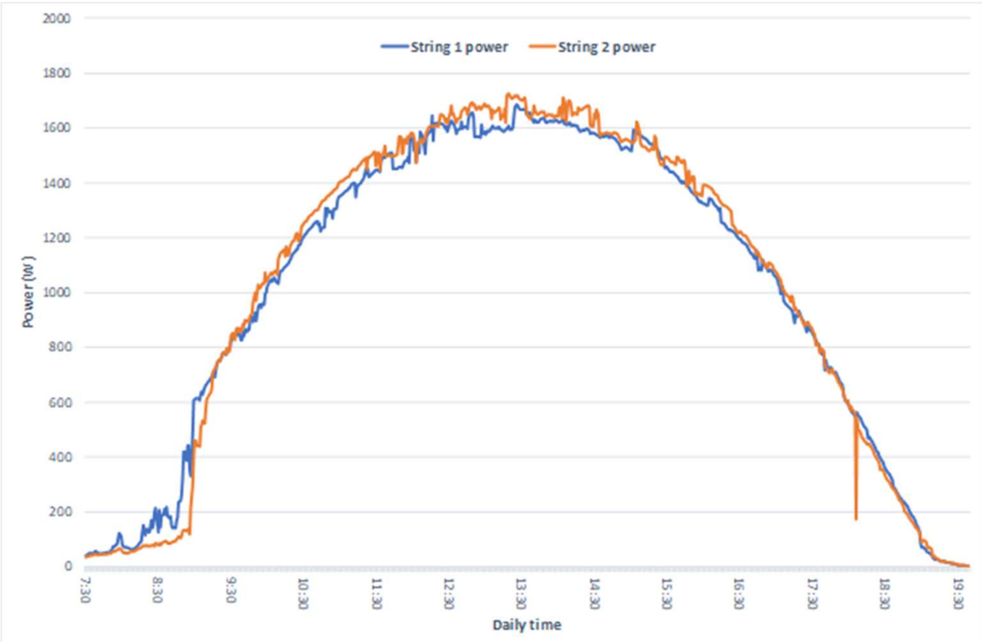

Figure 5: Evolution of both strings power throughout a complete measured sunny day

Therefore, in the treatment of the data, the values of the sunny day have been filtered in order to use the data collected from 9:30 a.m. to 7:30 p.m.

Finding the lack of homogeneity existing in the albedo radiation incident on the installation [37], it has been decided to make a power estimation analysis using a theoretical model applied to BPV modules for a sunny day and a cloudy day using equation 3 [39], [40].

$$P_A = P_0 \times \frac{G_E}{G_{ref}} \times [1 + \gamma\,(T_m - 25^{o}C)] \quad (3)$$

Where G_E is the equivalent irradiance composed defined in [28].

Each array is connected in series and each module receives different irradiance so, the current of each string is limited to that of the module with the lowest production. Therefore, a theoretical power delivered has been calculated assuming that the rear irradiance received is that of each sensor in order to observe the discrepancies between each theoretical power curve and the actual power measured. The analysis has been carried out independently for the power of string 1, the power of string 2 and the total power of the system.

Figure 6 represents a dispersion of the values estimated by each sensor for each minute of the day with respect to the actual measured power of string 1 for a sunny day and a cloudy day.

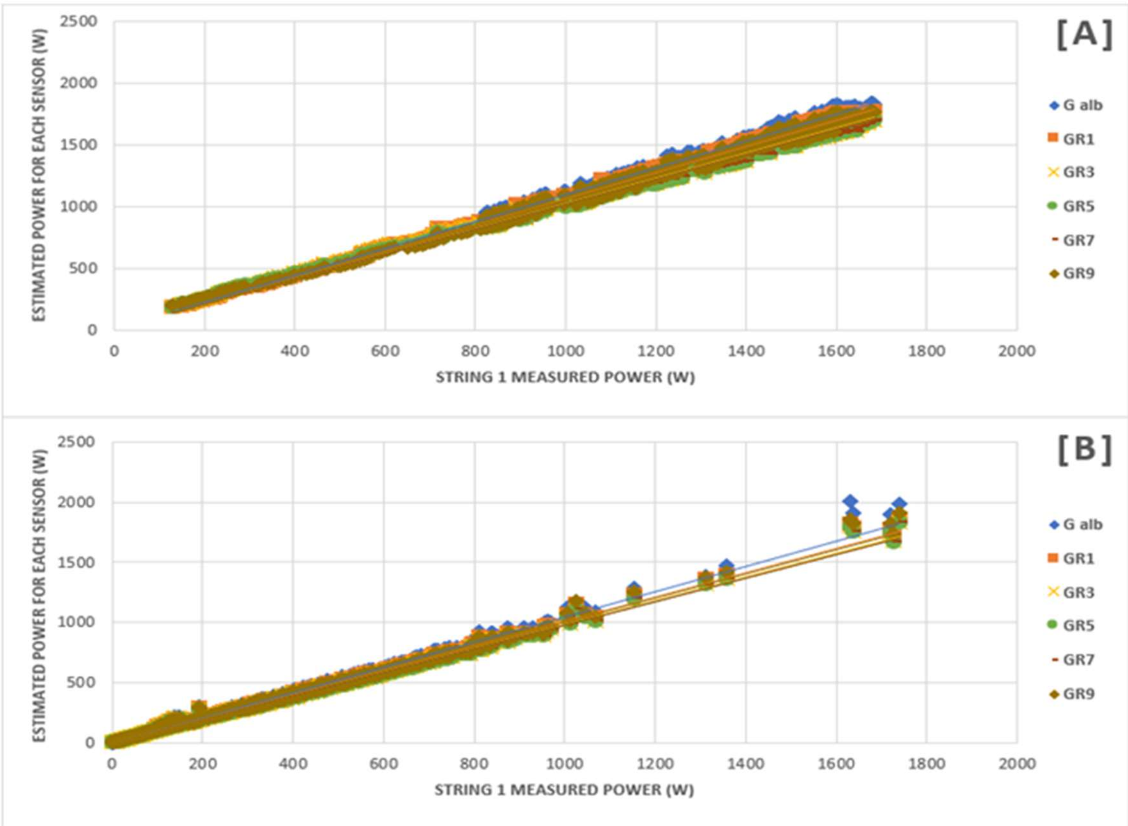

Figure 6: Dispersion of power estimation values vs measured power of the string 1. [A] On a sunny day. [B] On a cloudy day

Figure 7 shows the dispersion of the values of the estimated powers for string 2 against the actual power measured for a sunny day and a cloudy day

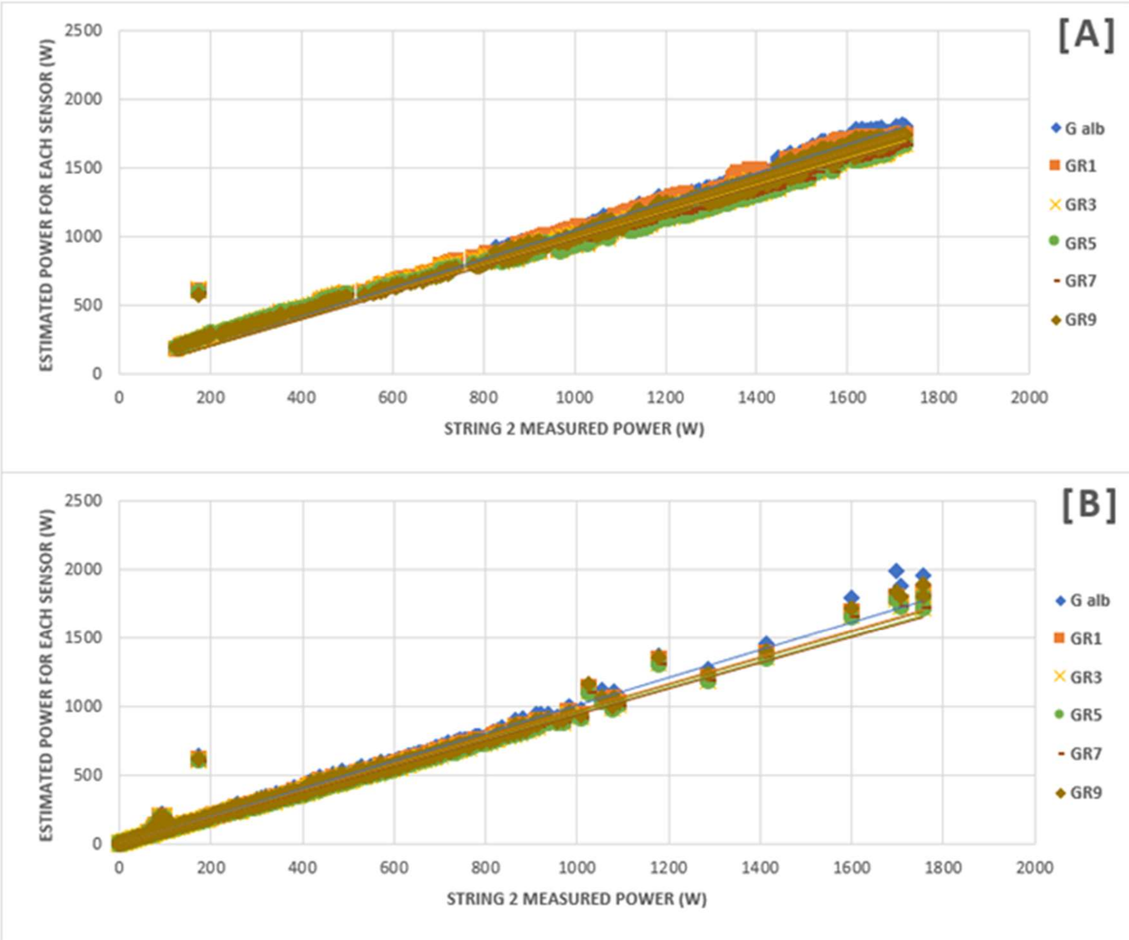

Figure 7: Dispersion of power estimation values vs measured power of the string 2. [A] On a sunny day. [B] On a cloudy day

Figure 8 shows the dispersion of the values of the estimated powers for the total system against the actual power measured for a sunny day and a cloudy day.

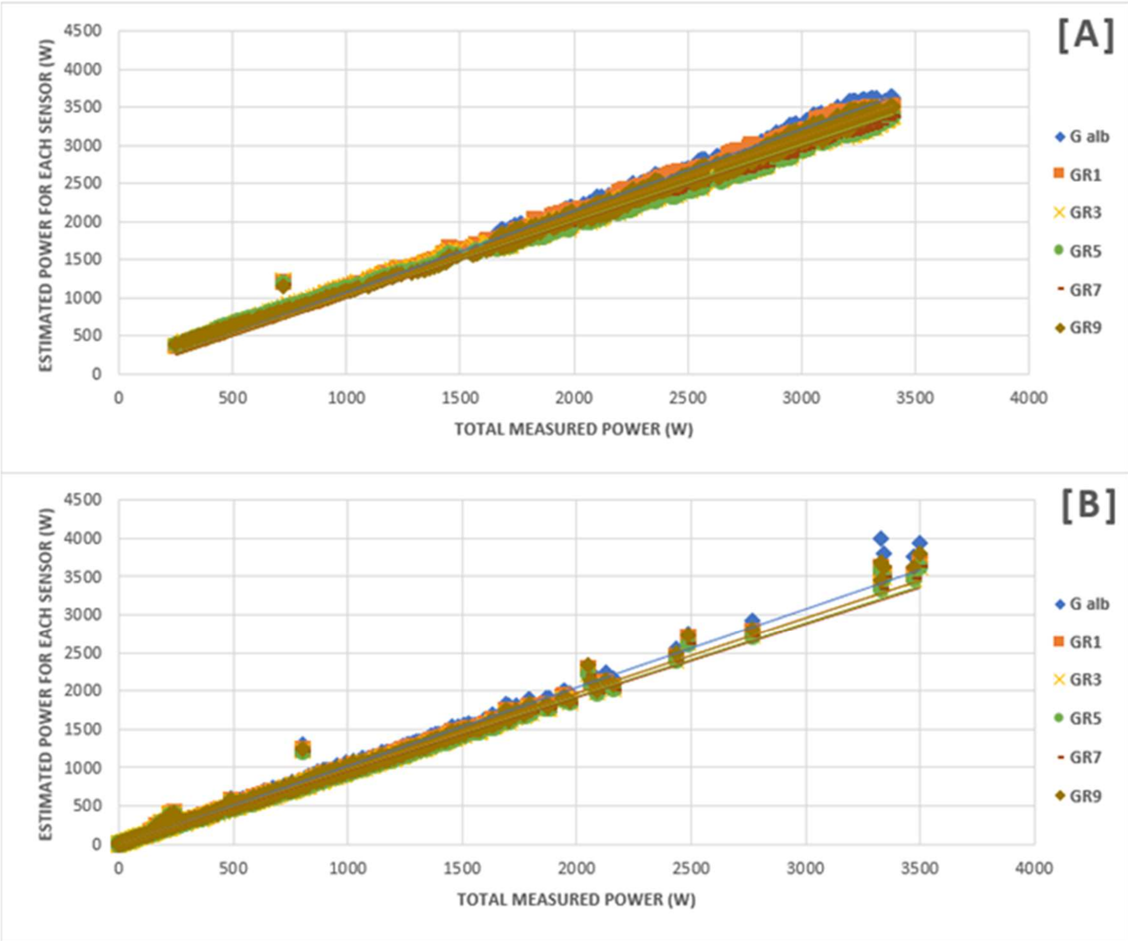

Figure 8: Dispersion of power estimation values vs measured power of the total system. [A] On a sunny day. [B] On a cloudy day

The estimated data have linear trends with respect to the actual power measured. Tables 4 and 5 represent the linear fit coefficients for the power estimated by each sensor, as well as the R^2 index that evaluates the accuracy of the adjustment.

Table 4: Linear fit coefficients for the estimated power value by each sensor on a sunny day

		Galb	GR1	GR3	GR5	GR7	GR9
String 1	**Fit coefficient**	1.094	1.059	1.023	1.019	1.018	1.057
	R^2	0.994	0.990	0.993	0.994	0.995	0.993
String 2	**Fit coefficient**	1.048	1.015	0.980	0.976	0.975	1.013
	R^2	0.995	0.988	0.990	0.991	0.992	0.994
Total	**Fit coefficient**	1.071	1.037	1.001	0.998	0.996	1.035
	R^2	0.995	0.987	0.991	0.992	0.993	0.994

Table 5: Linear fit coefficients for the estimated power value by each sensor on a cloudy day

		Galb	GR1	GR3	GR5	GR7	GR9
String 1	**Fit coefficient**	1.045	1.007	0.983	0.980	0.977	1.004
	R^2	0.995	0.997	0.994	0.996	0.996	0.995
String 2	**Fit coefficient**	1.006	0.970	0.946	0.943	0.941	0.966
	R^2	0.989	0.991	0.991	0.991	0.991	0.990
Total	**Fit coefficient**	1.026	0.989	0.965	0.962	0.959	0.985
	R^2	0.993	0.996	0.995	0.995	0.995	0.994

In general, it is detected that the main difference found between sunny and cloudy days is that the accuracy of the estimated power adjustment with each sensor is more uniform in the case of cloudy days. In the case of the sunny day, there is greater precision for the adjustment of the estimated power with the GR5 and GR7 sensors.

To ensure the validity of the results, the mean square error index (RMSE) has been used as shown in equation 4:

$$\boldsymbol{RMSE} = \frac{\sqrt{\frac{\sum(\boldsymbol{P_{measured}} - \boldsymbol{P_{estimated}})^2}{\boldsymbol{N}}}}{\frac{\sum \boldsymbol{P_{measured}}}{\boldsymbol{N}}} \ (\%) \qquad (4)$$

The trends in the results of the application of the above equation are shown in Figure 9.

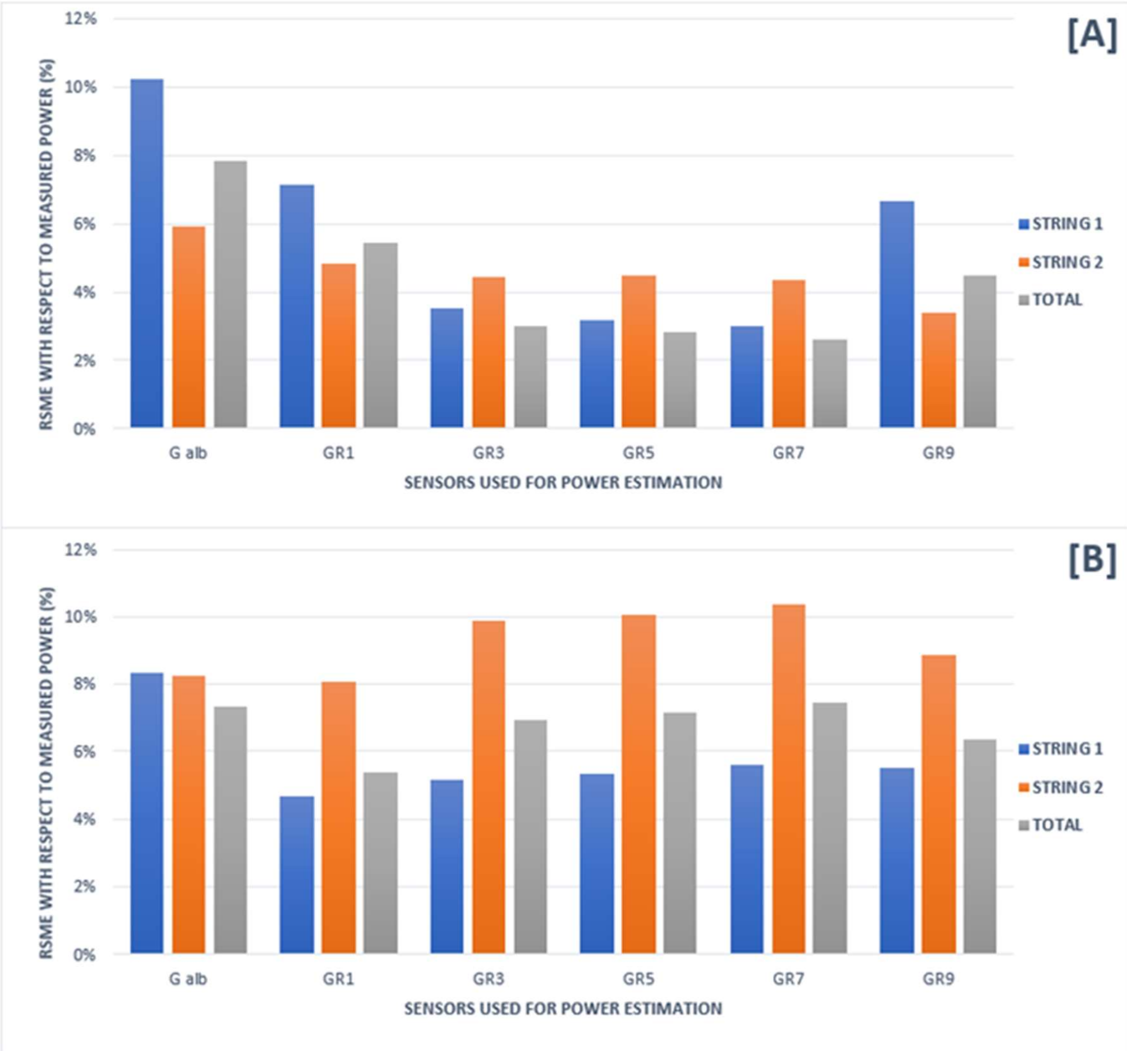

Figure 9: RMSE committed on the power estimation by each sensor with respect to the measured power. [A] On a sunny day. [B] On a cloudy day

On the sunny day, in the case of the error in the estimated power for string 1, it is verified that it has a parabolic behaviour according to the position of the sensors, reaching values below 5% for the central sensors of the array. However, regarding the estimated power for string 2, it is observed that it does not share the same behaviour, but that the error tends to be more linear. The rear irradiance maps represented in the previous section shows the evolution of irradiance along an array that occupies the space of nine modules, however, string 2 is composed of two rows of only two modules. Based on this map, we can corroborate that the homogeneity of the rear irradiance of string 2 is greater than that of string 1 and, therefore, there is a greater error in the power estimate of string 2, but more constant.

Regarding the cloudy day, it is observed in general that there is greater error in the estimation of power, but less difference between the estimates of the sensors, corroborating the greater homogeneity existing in cloudy days than in sunny days.

Tables 6 and 7 represent the numerical data corresponding to the calculated mean square errors.

Table 6: RMSE rated values committed on the power estimation with respect to the measured power on a sunny day

	RMSE					
	G alb	**GR1**	**GR3**	**GR5**	**GR7**	**GR9**
STRING 1	10.22%	7.13%	3.54%	3.16%	2.98%	6.65%
STRING 2	5.92%	4.85%	4.45%	4.48%	4.35%	3.40%
TOTAL	7.84%	5.44%	3.02%	2.83%	2.63%	4.50%

Table 7: RMSE rated values committed on the power estimation with respect to the measured power on a cloudy day

	RMSE					
	G alb	**GR1**	**GR3**	**GR5**	**GR7**	**GR9**
STRING 1	8.33%	4.66%	5.17%	5.35%	5.58%	5.51%
STRING 2	8.24%	8.06%	9.87%	10.08%	10.36%	8.85%
TOTAL	7.34%	5.40%	6.95%	7.17%	7.45%	6.35%

In order to obtain a representative sensor that allows an estimate of the total power of the system, it is observed that on a sunny day we find from the GR5 to the GR7 sensor less than 3%, which indicates that they could offer relatively reliable production simulation data.

3.4 Evaluation of the performance of the system

After collecting data from the entire experimental campaign, the following performance indices and metrics have been calculated applied to the DC part, encompassing the entire installation as a whole, obtaining a monthly daily average and then a daily average of the entire experimental campaign, following the IEC61724-1 [31] standard.

The yield of the photovoltaic array has been calculated, following equation 5:

$$\boldsymbol{Y_A = \sum_k \frac{P_{A,k} \times \tau_k}{P_0} = \frac{E_A}{P_0}} \quad (5)$$

Where the product of the power output of the array ($P_{A,k}$) and the time of the measuring period (τ_k) results in the energy output of the array (E_A) and P_0 represents the rated power value of the array.

The reference yield has been obtained by dividing the total front irradiation (H_i) over the STC irradiance ($G_{i,ref}$), as shown in equation 6, whereas the bifacial reference yield has been calculated using equation 7:

$$\boldsymbol{Y_r = \frac{H_i}{G_{i,ref}}} \quad (6)$$

$$\boldsymbol{Y_r^{bi} = \sum_k \frac{G_{i,k} \times \tau_k \times BIF_k}{G_{i,ref}}} \quad (7)$$

In the numerator in equation 7, the product of the front irradiance ($G_{i,k}$) and the bifacial irradiance factor (BIF_k) represents the equivalent irradiance incident in the bifacial module, that has been multiplied by the time of each measuring period (τ_k) in order to obtain the total equivalent irradiation for bifacial modules.

It has made use of the PR index, calculated with equation 8, adapted to bifacial conditions by applying the relationship between frontal and posterior irradiance BIF:

$$PR^{bi} = \frac{\sum_k \frac{P_{A,k} \times \tau_k}{P_0}}{\sum_k \frac{G_{i,k} \times BIF_k \times \tau_k}{G_{i,ref}}} = \frac{Y_A}{Y_r^{bi}} \quad (8)$$

Finally, the PR index has been normalized through equation 9 by applying a correction coefficient in temperature ($C_{k,25ºC}$), explained in equation 10, to obtain the temperature equivalent index of standard measurement conditions:

$$PR_{25ºC}^{bi\prime} = \frac{\sum_k \frac{P_{A,k} \times \tau_k}{P_0 \times C_{k,25ºC}}}{\sum_k \frac{G_{i,k} \times BIF_k \times \tau_k}{G_{i,ref}}} = \frac{Y_{A,25ºC}}{Y_r^{bi}} \quad (9)$$

$$C_{k,25ºC} = 1 + \gamma \times (T_{mod,k} - 25ºC) \quad (10)$$

Where $T_{mod,k}$ is the measured module temperature for each measurement period.

The realization of this analysis aims to show a real vision of how performance metrics can vary depending on the position and the type of sensor used for the measurement of the rear irradiance.

As a second consideration, the evaluation has been carried out in one case with the nominal parameters offered by the manufacturer and in another with the nominal parameters measured in the characterization campaign. Figure 10 shows the average daily array and reference yields, both monthly daily average and global campaign average.

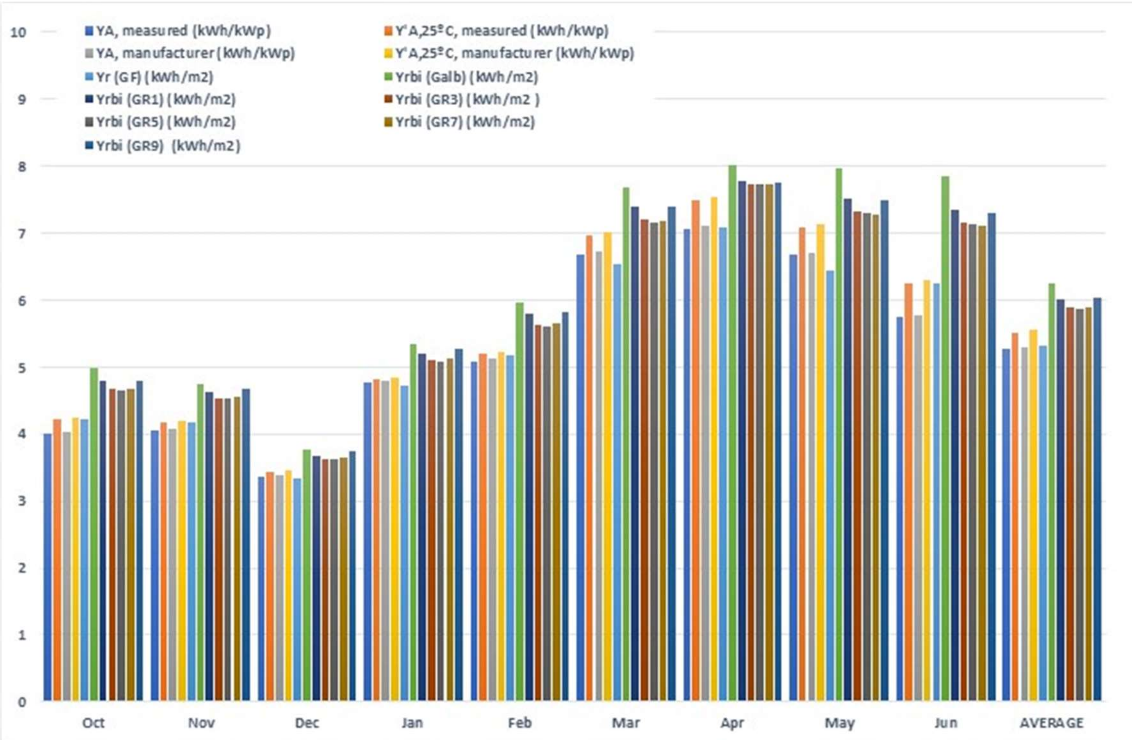

Figure 10: Monthly daily average and total experimental campaign average values of the different array yields calculated, the frontal reference yield and the bifacial reference yield of each rear sensor

The Figure 11 show the monthly daily averages and the global daily average of the PR calculated with each sensor.

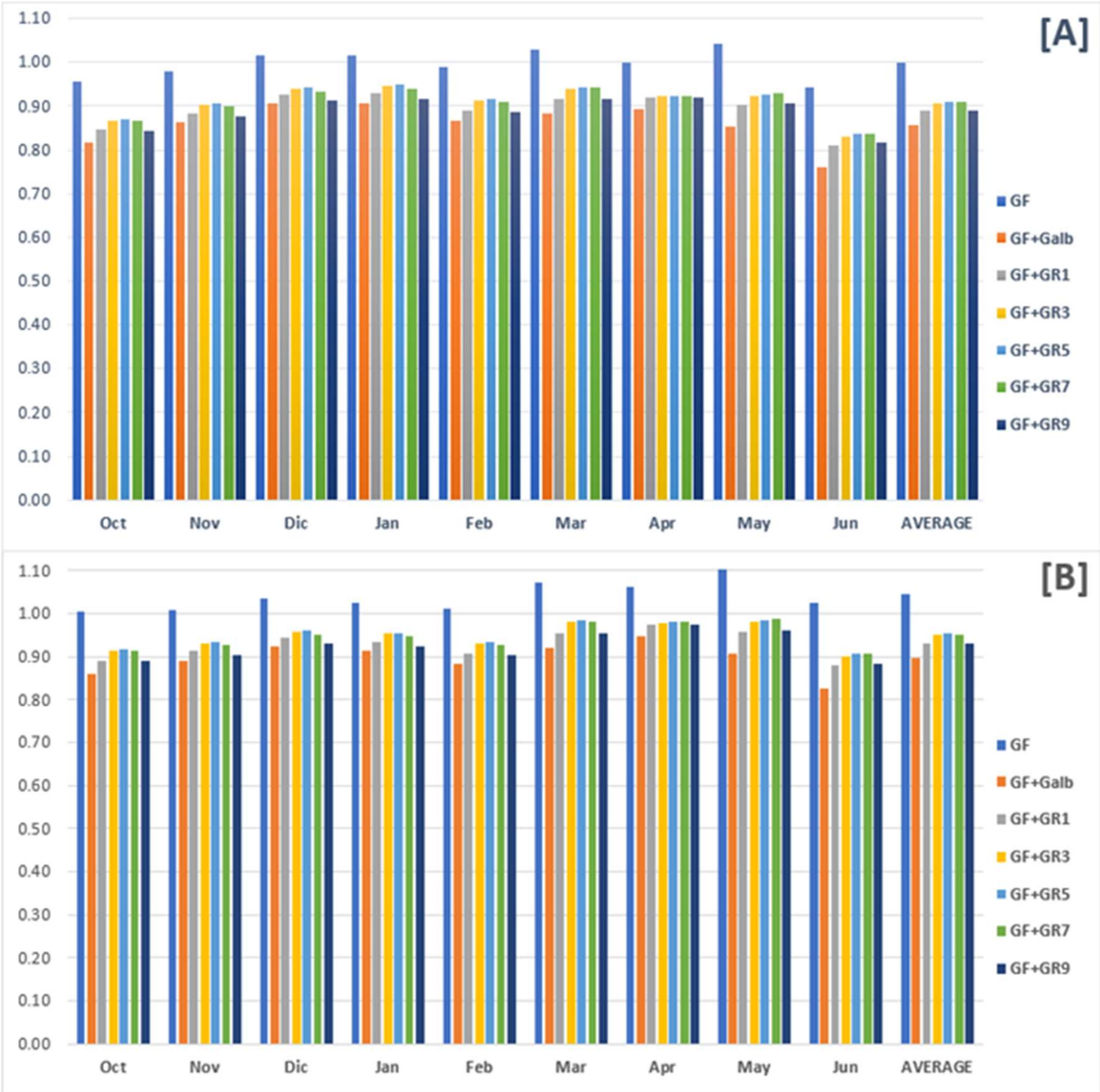

Figure 11: Monthly daily PR average and total experimental campaign daily PR average using measured rated values. [A] Using measured energy values. [B] Using temperature-corrected energy values to 25ºC

Using only frontal irradiation for its calculation, the values are close to or greater than 1 when considering bifacial energy production, but only with respect to frontal irradiation

without counting rear albedo irradiation. As for the PR calculated with the frontal irradiation and some sensor that measures rear irradiation, the following is detected:
On the one hand, using the albedometer, the lowest value is obtained since, as observed in the power estimation, it measures more irradiation than any sensor and differs greatly from what the module actually converts. On the other hand, paying attention to the values calculated with the sensors of string 1, there is a clear trend in which the lower PR's occur with the extreme sensors and increases as the sensor is more focused on the string centre. Figure 12 presents the global averages of each type of PR calculated for each sensor.

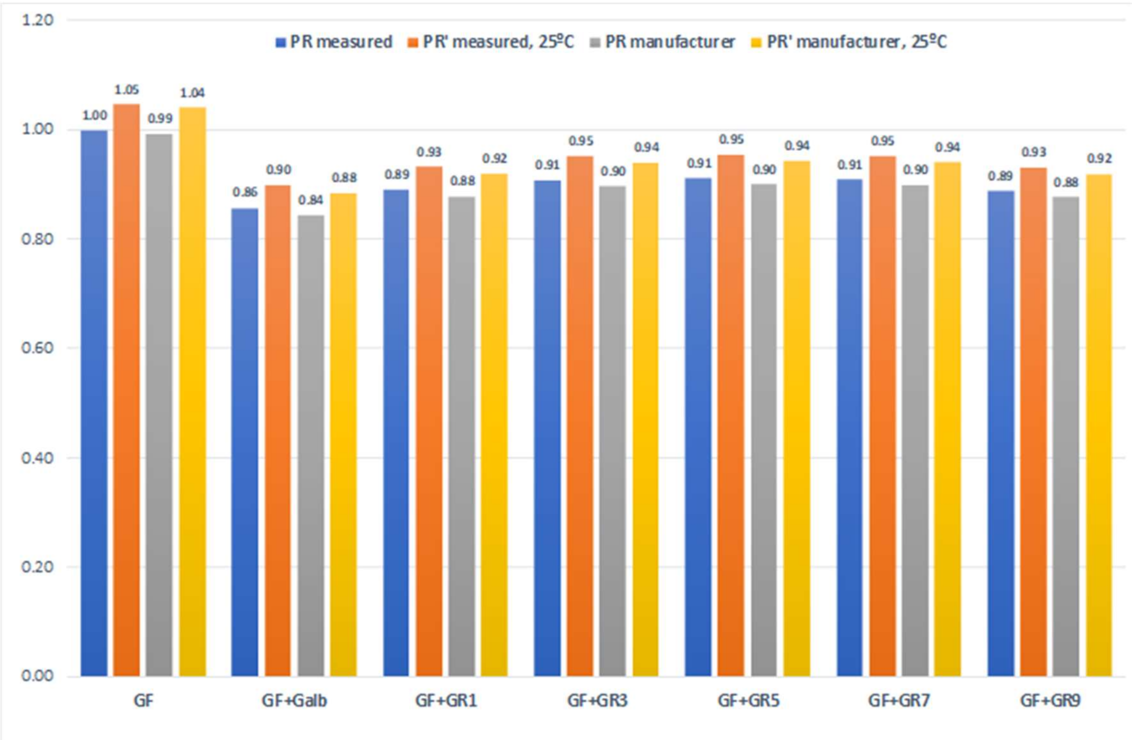

Figure 12: Total experimental campaign daily average comparison between different types of PR calculated by each sensor

The differences between the PR calculated using the parameters measured in the characterization campaign and the manufacturer's parameters are scarce, but favourable to the use of the measured parameters. Whereas, the PR corrected at STC temperature does differ quite a bit from the PR without temperature correction.

4. CONCLUSIONS

As a first noteworthy conclusion, it is important to carry out a previous campaign of characterization and calibration of modules and instruments in order to obtain more reliable results in the analyses carried out. Moreover, it can allow to make a BPV modules degradation research in the future.

The rear irradiance map has determined the differences between the measurements of the different rear irradiance sensors along a string that occupies the space of nine modules with a GNU of up to 35%. Thanks to this map it is possible to estimate the homogeneity differences that can exist in a string of shorter length. In other hand, large photovoltaic systems trend to have longer strings than the nine string modules analysed, so the results of the irradiance map suggest that the larger the array, the more homogeneous irradiance will be in the central part.

In the analysis of estimation of daily power, the effects of the lack of homogeneity are reflected, where the RMSE of the estimated power with respect to the real one has varied between 10.22% and 2.63%. The results of the power estimation show dependence on the position of the sensor with which the prediction is made and the configuration of the string on which it is made. In arrays of shorter length, the rear irradiance is more homogeneous than in arrays of greater length, therefore, the value of effective back irradiance obtained in configurations of shorter length may be higher than in configurations of greater length.

Regarding the behaviour on cloudy days, although the error in the calculation is greater, it is more linear in reference to the different sensor configurations, which indicates that the rear irradiance has an important diffuse component, making it more homogeneous.

Finally, after evaluating the photovoltaic system through the goodness indexes, the difference between the possible values that can be obtained from the PR has been seen depending on whether the normalized PR is calculated at STC temperature and the location of the rear irradiance sensor. Therefore, it is concluded that, in the case of a contract for a bifacial photovoltaic installation in which there is a clause that ensures a minimum PR value, it is important to define how this index will be measured and the position occupied by the irradiance sensors.

BIBLIOGRAPHY AND REFERENCES

[1] N. R. Furr and K. M. Eisenhardt, 'Strategy and Uncertainty: Resource-Based View, Strategy-Creation View, and the Hybrid Between Them', *J Manage*, vol. 47, no. 7, pp. 1915–1935, Sep. 2021, doi: 10.1177/01492063211011760.

[2] J. Chilvers *et al.*, 'Realising transition pathways for a more electric, low-carbon energy system in the United Kingdom: Challenges, insights and opportunities', *Proceedings of the Institution of Mechanical Engineers, Part A: Journal of Power and Energy*, vol. 231, no. 6, pp. 440–477, Sep. 2017, doi: 10.1177/0957650917695448.

[3] VDMA, 'International Technology Roadmap for Photovoltaic', *2022 Results*, vol. 14th Edition, 2023.

[4] J. Eguren, F. Martínez-Moreno, P. Merodio, and E. Lorenzo, 'First bifacial PV modules early 1983', *Solar Energy*, vol. 243, pp. 327–335, Sep. 2022, doi: 10.1016/J.SOLENER.2022.08.002.

[5] A. Cuevas, A. Luque, J. Eguren, and J. del Alamo, '50 Per cent more output power from an albedo-collecting flat panel using bifacial solar cells', *Solar Energy*, vol. 29, no. 5, pp. 419–420, Jan. 1982, doi: 10.1016/0038-092X(82)90078-0.

[6] M. Vimala, G. Ramadas, M. Perarasi, A. M. Manokar, and R. Sathyamurthy, 'A Review of Different Types of Solar Cell Materials Employed in Bifacial Solar Photovoltaic Panel', *Energies*, vol. 16, no. 8. MDPI, Apr. 01, 2023. doi: 10.3390/en16083605.

[7] H. Deng *et al.*, 'Novel symmetrical bifacial flexible CZTSSe thin film solar cells for indoor photovoltaic applications', *Nat Commun*, vol. 12, no. 1, 2021, doi: 10.1038/s41467-021-23343-1.

[8] S. Ašmontas and M. Mujahid, 'Recent Progress in Perovskite Tandem Solar Cells', *Nanomaterials*, vol. 13, no. 12, p. 1886, Jun. 2023, doi: 10.3390/nano13121886.

[9] C. D. Rodríguez-Gallegos, M. Bieri, O. Gandhi, J. P. Singh, T. Reindl, and S. K. Panda, 'Monofacial vs bifacial Si-based PV modules: Which one is more cost-effective?', *Solar Energy*, vol. 176, pp. 412–438, Dec. 2018, doi: 10.1016/J.SOLENER.2018.10.012.

[10] E. Türkdoğru and M. Kutay, 'Analysis of albedo effect in a 30-kW bifacial PV system with different ground surfaces using PVSYST software', *Journal of Energy Systems*, vol. 6, no. 4, pp. 543–559, 2022, doi: 10.30521/jes.1105348.

[11] X. Sun, M. R. Khan, C. Deline, and M. A. Alam, 'Optimization and performance of bifacial solar modules: A global perspective', *Appl Energy*, vol. 212, pp. 1601–1610, Feb. 2018, doi: 10.1016/J.APENERGY.2017.12.041.

[12] J. E. Castillo-Aguilella and P. S. Hauser, 'Multi-Variable Bifacial Photovoltaic Module Test Results and Best-Fit Annual Bifacial Energy Yield Model', *IEEE Access*, vol. 4, pp. 498–506, 2016, doi: 10.1109/ACCESS.2016.2518399.

[13] A. Tuomiranta, P.-J. Alet, C. Ballif, and H. Ghedira, 'Calibration of ground surface albedo models', *Solar Energy*, vol. 237, pp. 239–252, 2022, doi: 10.1016/j.solener.2022.03.047.

[14] Z. Er and E. Balci, 'Dual axis solar angle tracking system without any sensor', *Journal of Energy Systems*, vol. 2, no. 3, pp. 127–136, 2018, doi: 10.30521/JES.456606.

[15] C. Alexandru and C. Pozna, 'Simulation of a dual-axis solar tracker for improving the performance of a photovoltaic panel', *Proceedings of the Institution of Mechanical Engineers, Part A: Journal of Power and Energy*, vol. 224, no. 6, pp. 797–811, Jan. 2010, doi: 10.1243/09576509JPE871.

[16] V. Durković and Đurišić, 'Extended model for irradiation suitable for large bifacial PV power plants', *Solar Energy*, vol. 191, pp. 272–290, 2019, doi: 10.1016/j.solener.2019.08.064.

[17] B. Sun, L. Lu, Y. Yuan, and P. Ocłoń, ‘Development and validation of a concise and anisotropic irradiance model for bifacial photovoltaic modules’, *Renew Energy*, vol. 209, pp. 442–452, 2023, doi: 10.1016/j.renene.2023.04.012.

[18] A. Ghosh, ‘A comprehensive review of water based PV: Flotavoltaics, under water, offshore & canal top’, *Ocean Engineering*, vol. 281, p. 115044, Aug. 2023, doi: 10.1016/J.OCEANENG.2023.115044.

[19] G. M. Tina, F. Bontempo Scavo, L. Merlo, and F. Bizzarri, ‘Comparative analysis of monofacial and bifacial photovoltaic modules for floating power plants’, *Appl Energy*, vol. 281, p. 116084, Jan. 2021, doi: 10.1016/J.APENERGY.2020.116084.

[20] L. Djordjevicć *et al.*, ‘Increasing Energy Efficiency of Buildings in Serbia—A Case of an Urban Neighborhood’, *Sustainability (Switzerland)*, vol. 15, no. 7, Apr. 2023, doi: 10.3390/su15076300.

[21] S. Gulkowski, ‘Specific Yield Analysis of the Rooftop PV Systems Located in South-Eastern Poland’, *Energies (Basel)*, vol. 15, no. 10, May 2022, doi: 10.3390/en15103666.

[22] E. A. Al-Sharafi, M. Alhussein, A. Ali, and K. Aurangzeb, ‘Rooftop Solar PV Policy Assessment of Global Best Practices and Lessons Learned for the Kingdom of Saudi Arabia’, *Sustainability*, vol. 15, no. 12, p. 9630, Jun. 2023, doi: 10.3390/su15129630.

[23] Y. Kim, Y. On, J. So, S. Kim, and S. Kim, ‘A Decision Support Software Application for the Design of Agrophotovoltaic Systems in Republic of Korea’, *Sustainability (Switzerland)*, vol. 15, no. 11, Jun. 2023, doi: 10.3390/su15118830.

[24] Y. de J. Acosta-Silva *et al.*, ‘Applications of solar and wind renewable energy in agriculture: A review’, *Sci Prog*, vol. 102, no. 2, pp. 127–140, Jun. 2019, doi: 10.1177/0036850419832696.

[25] E. Mouhib, L. Micheli, F. M. Almonacid, and E. F. Fernández, ‘Overview of the Fundamentals and Applications of Bifacial Photovoltaic Technology: Agrivoltaics and Aquavoltaics’, *Energies*, vol. 15, no. 23. MDPI, Dec. 01, 2022. doi: 10.3390/en15238777.

[26] D. Cabral, A. Hayati, J. Gomes, H. A. Gorouh, P. Nasseriyan, and M. Salmanzadeh, 'Experimental Electrical Assessment Evaluation of a Vertical n-PERT Half-Size Bifacial Solar Cell String Receiver on a Parabolic Trough Solar Collector', *Energies (Basel)*, vol. 16, no. 4, Feb. 2023, doi: 10.3390/en16042007.

[27] I. D. Fajuke and A. K. Raji, 'Firefly Algorithm-Based Optimization of the Additional Energy Yield of Bifacial PV Modules', *Energies (Basel)*, vol. 15, no. 7, Apr. 2022, doi: 10.3390/en15072651.

[28] J. S. Stein and G. Friesen, *IEA PVPS Task 13 Performance, Operation and Reliability of Photovoltaic Systems-Bifacial Photovoltaic Modules and Systems: Experience and Results from International Research and 2.707) on 'Increasing the Lifetime of Photovoltaics Systems: Advanced Materials, Monitoring, O&M and Energy Modeling' View project*. [Online]. Available: www.iea-pvps.org

[29] IEC TS 60904-1-2, *Photovoltaic devices-Part 1-2: Measurement of current-voltage characteristics of bifacial photovoltaic (PV) devices*. 2019. [Online]. Available: www.iec.ch

[30] J. Lopez-Garcia *et al.*, 'Implementation of the IEC TS 60904-1-2 Measurement Methods for Bifacial Silicon PV Devices', *IEEE J Photovolt*, vol. 12, no. 3, pp. 787–797, 2022, doi: 10.1109/JPHOTOV.2022.3161186.

[31] IEC 61724-1, 'Photovoltaic system performance-Part 1: Monitoring', 2021. [Online]. Available: www.iec.ch

[32] P. K. Sahu, J. N. Roy, C. Chakraborty, and S. Sundaram, 'A new model for estimation of energy extraction from bifacial photovoltaic modules', *Energies (Basel)*, vol. 14, no. 16, Aug. 2021, doi: 10.3390/en14165089.

[33] N. H. Abdul Kahar, N. H. Azhan, I. Alhamrouni, M. N. Zulkifli, T. Sutikno, and A. Jusoh, 'Comparative analysis of grid-connected bifacial and standard mono-facial photovoltaic solar systems', *Bulletin of Electrical Engineering and Informatics*, vol. 12, no. 4, pp. 1993–2004, Aug. 2023, doi: 10.11591/eei.v12i4.5072.

[34] M. HASSAN ALI and A. MEHMOOD, 'Prognostic and Diagnostic Coupling Framework Based on OSA-CBM strategy for Photovoltaic Generators', *Journal of Polytechnic*, Jun. 2020, doi: 10.2339/politeknik.587253.

[35] Pulido López L, 'DISEÑO E IMPLEMENTACIÓN DE SISTEMAS DE MONITORIZACIÓN PARA LA CARACTERIZACIÓN DE TECNOLOGÍA BIFACIAL', Jaén, 2022.

[36] E. Caamaño, E. Lorenzo, and R. Zilles, 'Quality Control of Wide Collections of PV Modules: Lessons Learned from the IES Experience', Madrid, Spain, 1999.

[37] R. P. Kenny, E. Garcia Menendez, J. Lopez-Garcia, and B. Haile, 'Characterizing the operating conditions of bifacial modules', in *AIP Conference Proceedings*, American Institute of Physics Inc., Aug. 2018. doi: 10.1063/1.5049253.

[38] C. Rossa, F. Martínez-Moreno, and E. Lorenzo, 'Experimental observations in mismatch losses in monofacial and bifacial PV generators', *Progress in Photovoltaics: Research and Applications*, vol. 29, no. 12, pp. 1223–1235, Dec. 2021, doi: 10.1002/pip.3447.

[39] D. L. Evans, 'SIMPLIFIED METHOD FOR PREDICTING PHOTOVOLTAIC ARRAY OUTPUT', *Solar Energy*, vol. 27, no. 6, pp. 555–560, 1981.

[40] C. R. Osterwald, 'TRANSLATION OF DEVICE PERFORMANCE MEASUREMENTS TO REFERENCE CONDITIONS*', 1986.

FUNDING

The realization of the experiments that has made possible the redaction of this article has been carried out thanks to the support of two projects:

"Optimized models for the energy characterization of grid-connected photovoltaic systems with bifacial technology" (Ref 1380734), funded by the European Union (FEDER).

"Modelling the performance of bifacial PV systems integrated in Smart-Trees using Deep Learning Techniques" (TED2021-131983B-100 ENE), funded by the Spanish Ministry of Science and Innovation with the program Projects Oriented to the Ecological Transition and the Digital Transition (Call 2021).

INDEX OF NOMENCLATURE AND ABBREVIATION

LCOE	Levelized cost of energy
PR	Performance ratio
$PR_{25ºC}$	Performance ratio standardized to 25ºC
BPV	Bifacial photovoltaic
MPPT	Maximum power point tracker
STC	Standard test conditions
GNU	Irradiance non-uniformity index
P_A	Power output of the array (W)
G_E	Irradiance composed by frontal and rear irradiance (W/m^2)
T_m	Module operating temperature
RMSE	Root mean square error (%)
DC	Direct current
Y_A	Array yield
$Y_{A,\ 25ºC}$	Array yield translated to STC temperature
E_A	Energy output of the array (kWh)
$E_{A,\ 25ºC}$	Energy output of the array translated to STC temperature
P_0	Rated power value
Y_r	Reference yield
Y_r^{bi}	Bifacial reference yield
G	Irradiance (W/m^2)
G_{ref}	Irradiance at STC (W/m^2)
H	Irradiation (kWh/m^2)
PR^{bi}	Bifacial performance ratio
BIF	Ratio between rear and frontal irradiance

LIST OF TABLES

LIST OF FIGURES